IEEE Access
Multidisciplinary | Rapid Review | Open Access Journal

Received August 3, 2021, accepted August 24, 2021, date of publication September 3, 2021, date of current version September 15, 2021.

Digital Object Identifier 10.1109/ACCESS.2021.3110210

Dual-Band Transmitter and Receiver With Bowtie-Antenna in 0.13 μm SiGe BiCMOS for Gas Spectroscopy at 222 - 270 GHz

KLAUS SCHMALZ[1], NICK ROTHBART[2,3], ALEXANDRA GLÜCK[2,3], MOHAMED HUSSEIN EISSA[1], (Member, IEEE), THOMAS MAUSOLF[1], ESREF TURKMEN[4,5], SELAHATTIN BERK YILMAZ[4], AND HEINZ-WILHELM HÜBERS[2,3]

[1]IHP—Leibniz-Institut für Innovative Mikroelektronik, 15236 Frankfurt (Oder), Germany
[2]Institute of Optical Sensor Systems, German Aerospace Center (DLR), 12489 Berlin, Germany
[3]Department of Physics, Humboldt-Universität zu Berlin, 12489 Berlin, Germany
[4]Silicon Radar GmbH, 15236 Frankfurt (Oder), Germany
[5]Institute of Radio Frequency and Electronics, Karlsruhe Institute of Technology, 76131 Karlsruhe, Germany

Corresponding author: Klaus Schmalz (schmalz@ihp-microelectronics.com)

This work was supported by Deutsche Forschungsgemeinschaft (DFG) through the DFG Project Elektromagnetische Sensoren für Life Sciences (ESSENCE) under Grant SPP 1857.

ABSTRACT This paper presents a transmitter (TX) and a receiver (RX) with bowtie-antenna and silicon lens for gas spectroscopy at 222-270 GHz, which are fabricated in IHP's 0.13 μm SiGe BiCMOS technology. The TX and RX use two integrated local oscillators for 222 – 256 GHz and 250 – 270 GHz, which are switched for dual-band operation. Due to its directivity of about 27 dBi, the single integrated bowtie-antenna with silicon lens enables an EIRP of about 25 dBm for the TX, and therefore a considerably higher EIRP for the 2-band TX compared to previously reported systems. The double sideband noise temperature of the RX is 20,000 K (18.5 dB noise figure) as measured by the Y-factor method. Absorption spectroscopy of gaseous methanol is used as a measure for the performance of the gas spectroscopy system with TX- and RX-modules.

INDEX TERMS Gas spectroscopy, mm-wave, SiGe, receiver, transmitter, bowtie antenna.

I. INTRODUCTION

High-resolution spectroscopy at millimeter-wave (mmW) /terahertz (THz) frequencies is a very powerful tool for gas sensing, because many molecules have rotational transitions in the mmW/THz range [1], [2], [3]. This technique can provide a profile of volatile organic compounds and toxic industrial chemicals in air [2], [3].

The recent development of components in SiGe BiCMOS or CMOS technology for applications at mmW/THz frequencies offers a path towards a compact and low-cost system for gas spectroscopy. Recently, a 220–320 GHz spectrometer has been described, which consists of a pair of 65 nm CMOS chips and utilizes two frequency-comb signals with ten equally spaced frequency tones to scan the spectrum [4], [5]. Furthermore, a transmitter (TX) and receiver (RX) in 65 nm CMOS have been reported [6]–[8], with gas spectroscopy results at 225 - 255 GHz, [9]. They were compared to results obtained by a solid state multiplier TX and RX made by Virginia Diodes Inc. (VDI) using GaAs Schottky diodes [10]. A 28 nm CMOS TX for pulsed operation at 180 GHz has been designed for in-situ molecular sensing in planetary science [11]. A complete 183 GHz CMOS/InP hybrid heterodyne-spectrometer with an InP low noise amplifier, a 28 nm CMOS RX and a 65 nm CMOS spectrometer have been recently realized for spaceborne atmospheric remote sensing applications [12]. Beyond molecular spectroscopy, wideband TXs and RXs as well as their sub-circuits for the range around 240 GHz are also required for high-bandwidth communication links, [13], [14]–[17], and high-resolution radar systems, [18], [19].

TXs and RXs, fabricated in IHP's 0.13 μm SiGe BiCMOS technology, with integrated antennas were demonstrated previously for gas spectroscopy at 238 - 252 GHz [20]–[22]. The design of the TX- and RX-circuits is described in detail in [23]–[26]. We also presented a compact TX/RX system with fractional-N phase-locked loops (PLLs), which allows frequency ramps for the TX and RX, as well as a

The associate editor coordinating the review of this manuscript and approving it for publication was Chan Hwang See.

superimposed frequency modulation using frequency shift keying (FSK) for the TX [27], [28].

The single-band TX/RX system was extended to a 2-band system to cover the range 225 - 273 GHz with two antennas [29]. A 2-band TX-chip and a 2-band RX-chip were reported, which were implemented by combining two TX- and two RX-circuits with their own on-chip antennas on corresponding single chips to realize an effective bandwidth of 222 - 270 GHz for our gas spectroscopy system [30]. LBE (Localized Backside Etching) technology, which is available at IHP, was used to realize on-chip antennas with high efficiency by removing the lossy silicon under the radiator. It was further shown that a RX with a mixer as first element has improved the performance of the spectroscopy system due to the higher linearity of the RX compared to a former RX in case of a 4xTX-array with high output power. We observed a lower signal-noise ratio (SNR) for gas spectroscopy by about a half when using a single TX with lower output power instead of the 4xTX-array (see [30]).

This paper describes the implementation of a single bowtie-antenna with silicon lens for a 2-band TX and RX to increase their performance parameters considerably compared to the previous 2-band TX and RX with two separate LBE on-chip antennas. A silicon-lens integrated planar antenna enables high antenna gain and a compact packaging solution (see e.g. [31]–[35]).

In the present paper, we will show that our TX/RX spectroscopy system provides a significantly higher sensitivity for high resolution gas spectroscopy compared to our previous systems. This results from the high directivity of the bowtie antenna with silicon lens and from using a single antenna for both channels which allows better alignment across the entire frequency band. The performance was demonstrated by the absorption spectra of gaseous methanol (CH_3OH).

The paper is organized as follows: The dual-band TX- and RX-chips with their bowtie-antenna with silicon lens for the TX/RX system are presented in Section II, followed by a presentation of system aspects and results of gas spectroscopy in Section III. Section IV provides a discussion of our results. The paper ends with the conclusion including an outlook concerning further improvement of our gas spectroscopy system.

II. TRANSMITTER AND RECEIVER

The TX and RX were implemented in SG13G2 technology, which is a 0.13 μm SiGe BiCMOS technology with very high bipolar performance of f_T/f_{max} = 300/500 GHz. This process provides two gate oxides: A thin gate oxide for the 1.2 V and a thick oxide for a 3.3 V supply voltage. For both modules NMOS and PMOS as well as isolated NMOS, transistors are offered. Further passive components like poly silicon resistors and MIM capacitors are available. The backend option offers five thin metal layers (Metal1 – Metal5), two thick metal layers TopMetal1 and TopMetal2 (2 and 3 μm thick), as well as MIM layer between Metal5 and TopMetal1, [36].

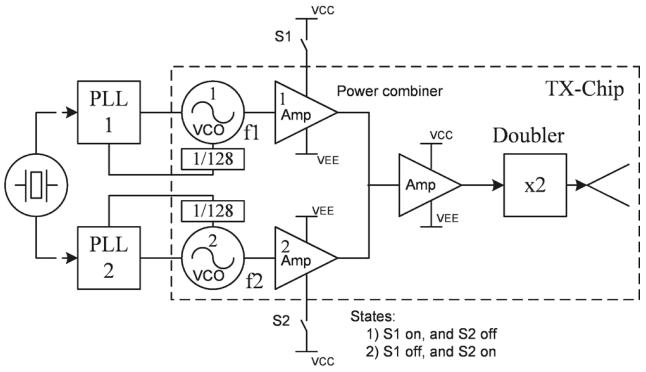

FIGURE 1. Block diagram of the 2-band TX with the two frequency ranges 222-256 GHz and 250-270 GHz.

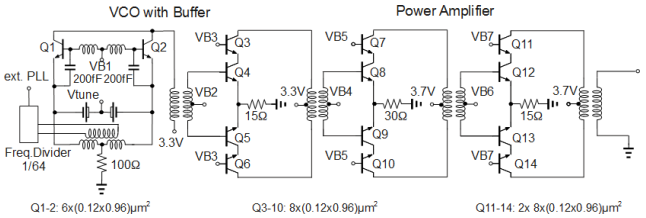

FIGURE 2. Schematic of the single-band LO for the two frequency ranges 111-128 GHz and 125-135 GHz determined by varactors of the VCO.

A. TRANSMITTER WITH 2-BAND LOCAL OSCILLATOR

Fig. 1 depicts the block diagram of the TX, whose single-ended output of the frequency doubler is connected to the differential bowtie-antenna by a balun.

The local oscillator (LO) consists of a push-push voltage controlled oscillator (VCO) with a frequency divider and a differential two stage power amplifier. The divider ratio of 1/128 is due to the 1/64 frequency divider applied for the fundamental frequency of the used push-push oscillator.

Fig. 2 depicts the schematic of the LO without details of the frequency divider. The LO-frequency is tuned by an external PLL. The push-push VCO is a harmonic oscillator, which consists of two sub-oscillators in common-collector topology. In the line to the supply-voltage, a transformer is placed, which transfers the signal to a differential cascode buffer with transformer-coupled output. We developed two VCOs for the two LOs with the following tuning ranges: 111 – 128 GHz and 125 −135 GHz.

The outputs of the two LOs are combined by a Wilkinson power combiner, which is connected through a power amplifier to a frequency doubler. The Wilkinson power combiner is implemented using microstrip lines. It is realized in the uppermost metal layer (TopMetal2) with a thickness of 3 μm. The ground layer is realized using Metal1, and the conductor width of the 50-Ohm transmission line is 16 μm. The Wilkinson power combiner was simulated with Momentum EM simulator. It exhibits an insertion loss of 1.5 dB at 120 GHz and more than 20 dB of isolation [22]. The power amplifier uses a transformer-coupled topology. The transistors of its first stage are scaled by a factor of 0.5. The power amplifier draws 55 mA

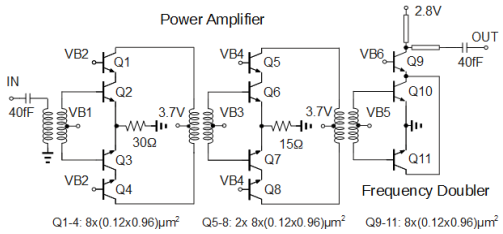

FIGURE 3. Schematic of the frequency doubler with 120 GHz amplifier.

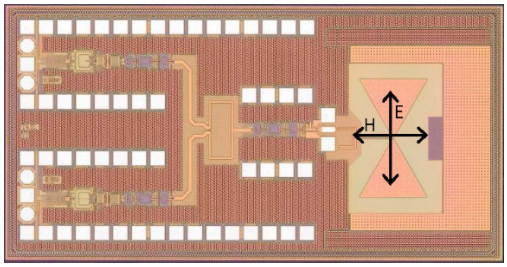

FIGURE 4. Photograph of the 2-band TX-chip (area: 2.64 × 1.34 mm^2, the arrows indicate the E- and H-plane of the antenna).

at 3.7 V supply voltage. Its measured gain is 19 dB at 120 GHz [37]. Fig. 3 shows the schematic of the frequency doubler connected to the two-stage power amplifier.

The frequency doubler has already been used in our previous TX- and RX-chips [30]. To avoid mixing the two LO-signals, only one LO is operating at a time, while the other one is switched off from its supply voltage electronically, and vice versa. This circuit block was also used for the dual-band RX, see below:

Fig. 4 shows the photograph of the dual-band TX-chip, whose area is of 2.64 × 1.34 mm^2.

B. RECEIVER WITH 2-BAND LOCAL OSCILLATOR

A mixer-first RX is implemented, with dc offset cancellation loop architecture to compensate for the mixer dc offsets and biasing purposes as described in [38]. A transimpedance amplifier (TIA) is utilized as a load for the mixer to maximize the bandwidth. The TIA input is regulated by a negative feedback biasing circuit to cancel the LO leakage and bias the mixer. This reported RX core (without internal LO) achieves a 3 dB bandwidth of 55 GHz, with a conversion gain of 13 dB. The noise figure (NF) was measured using the gain method, achieving an average single side band (SSB) NF of 18 dB [38].

Fig. 5 shows the measured conversion gain of the RX core at room temperature (25°C), the simulated conversion gain at different temperatures between 25°C and 70 °C, and the measured noise figure. The measured and simulated conversion gain at 25°C agree well.

Fig. 6 depicts the block diagram of the RX. The two LOs and their combination by a Wilkinson power combiner are described above. In the RX-chip the same frequency doubler was used as in the TX-chip. The frequency-doubled LO signal is then applied to the mixer, which is directly connected to

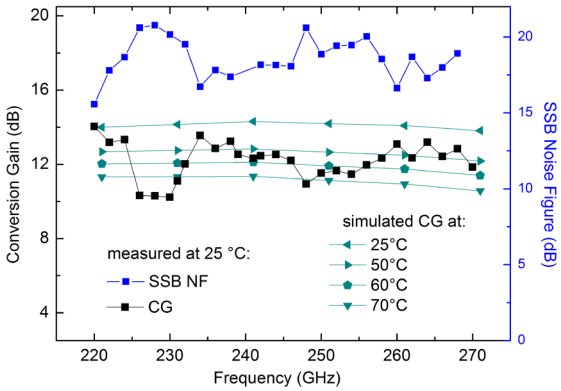

FIGURE 5. Measured conversion gain and noise figure of the RX core, and simulated conversion gain with temperature as parameter.

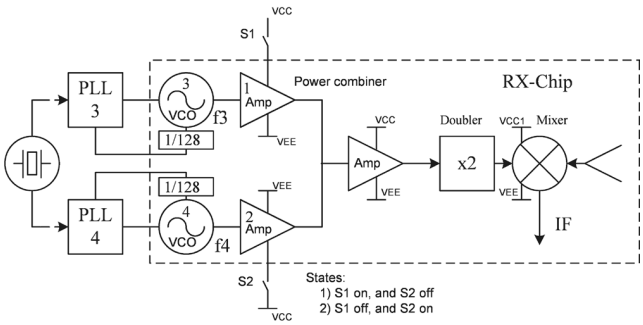

FIGURE 6. Block diagram of the 2-band receiver with two frequency ranges: 222-256 GHz and 250-270 GHz.

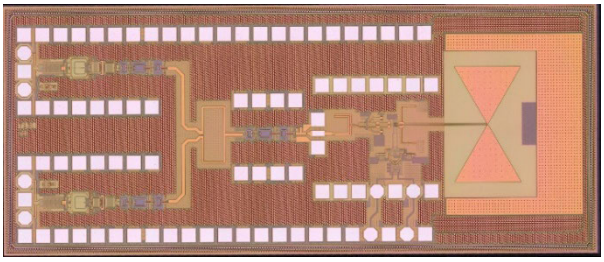

FIGURE 7. Photograph of the 2-band RX chip (area: 3.25 × 1.34 mm^2).

the differential bowtie-antenna. Fig. 7 shows the photograph of the dual-band RX-chip with an area of 3.25 × 1.34 mm^2.

C. BOWTIE ANTENNA WITH SILICON LENS

A linear polarized bowtie antenna is designed to satisfy the bandwidth requirement of the RX and TX front-end circuits.

The layout of the designed bowtie-antenna is shown in Fig. 8. The antenna is implemented using the top Al metallization layer (TopMetal2), which has a thickness of 3 μm. The metal frame around the bowtie structure is used to comply with the metal density rules of the SG13G2 design kit. The U-shaped part uses a layer stack including vias from Metal1 to TopMetal2. The straight metal stripe is created in Metal1. The antenna is optimized for backside radiation through the silicon substrate and silicon lens. The optimum bow angle and length (between the outer edges

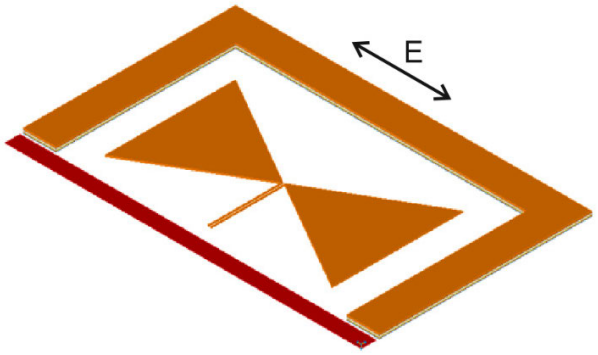

FIGURE 8. Layout of the designed bowtie antenna (TopMetal2 - ocher, Metal1 – red).

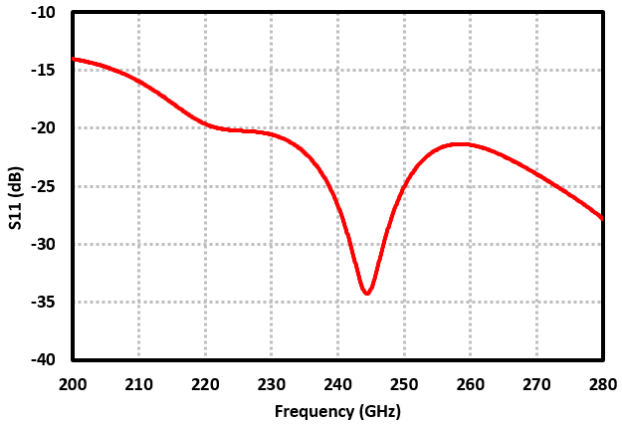

FIGURE 9. Simulated S11 of the bowtie-antenna.

of the two triangular parts) of the designed antenna are found as 60° and 632.6 μm, respectively. The size of the silicon lens is optimized by considering the trade-off between the beam-width and directivity. A hyper-hemispherical lens with a diameter of 10 mm and an extension of 1.4 mm is used without anti-reflection coating. The antenna with the silicon lens is simulated using a Finite Difference Time Domain (FDTD) based 3D EM field solver software, EMPIRE XPU.

Fig. 9 shows the S11 of the designed antenna. The simulated impedance bandwidth for a voltage standing wave ratio (VSWR) value less than 1.5 is more than 80 GHz. The antenna exhibits a total efficiency performance (radiated power over available power at input port) of about 65% over the frequency range of interest.

The simulated directivity is shown in Fig. 10. The designed antenna has a simulated directivity of 24.7 dBi with a 3 dB beam-width of 7.3° in horizontal polarization (H-plane) and 6° in vertical polarization (E-plane) at 240 GHz. Note that the metal frame does not influence the performance significantly. An antenna without this metal frame has a simulated directivity of 25.1 dBi with a 3 dB beam-width of 7.0° in horizontal polarization and 6° in vertical polarization at 240 GHz.

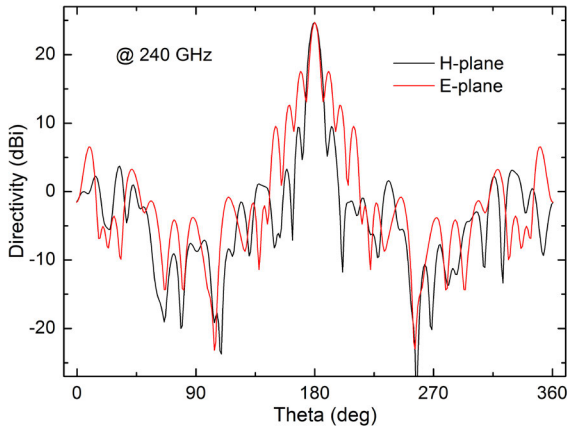

FIGURE 10. Simulated directivity of the bowtie-antenna at 240 GHz.

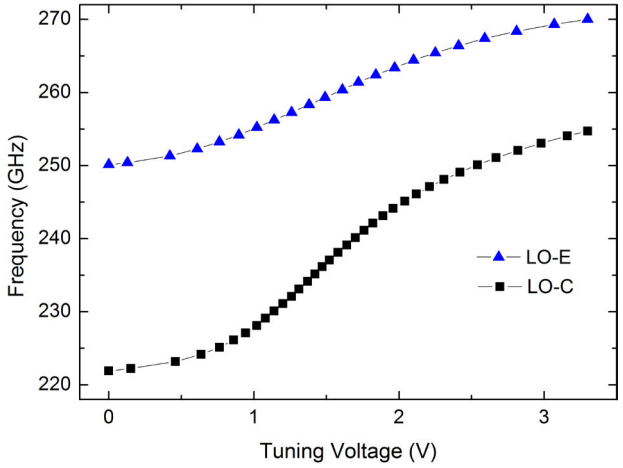

FIGURE 11. The measured frequency of the LO with frequency doubler is depicted as a function of the tuning voltage of its two VCOs. Two versions of LOs are realized for the two ranges 222-256 GHz and 250-270 GHz.

D. CHARACTERISTICS OF THE LOCAL OSCILLATORS

Fig. 11 shows the measured output frequencies of the two LOs for the frequency range 222-270 GHz as a function of the VCO tuning voltage. The two LOs are based on the same topology with optimized parameters for the following two frequency ranges: 222-256 GHz and 250-270 GHz.

Fig. 12 depicts the measured output power of the frequency doubler and the simulated one with temperature as parameter as a function of its output frequency. The output was obtained by on-wafer measurements of the 2-band RX using probes at the output of the frequency doubler (Fig. 7), while the supply voltages of the mixer were switched off, see Fig. 6. The frequency of the operating LO was set by adjusting the tuning voltage of VCO. Only one LO was operating during the measurement, while the other one was switched off by disconnecting its VCO, power amplifier, and frequency divider from their supply voltages, and vice versa. The results agree well with our previous results for a 2-band LO, which did include neither a Wilkinson power combiner nor a second power amplifier in front of the frequency doubler [30].

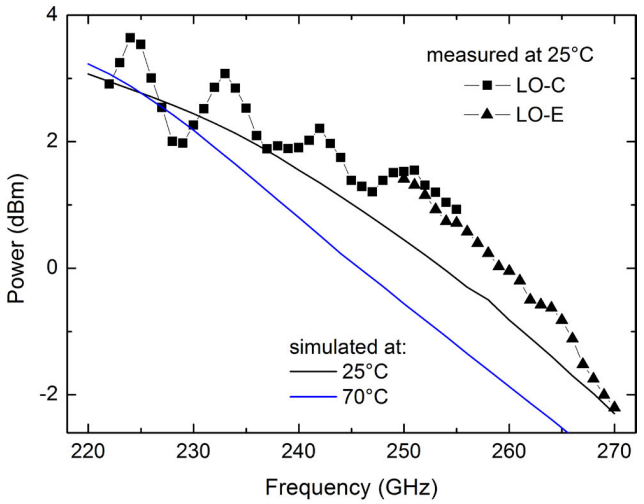

FIGURE 12. Measured output power of the LO with the frequency doubler plotted as function of the frequency of its two VCOs, and simulated power with temperature as parameter.

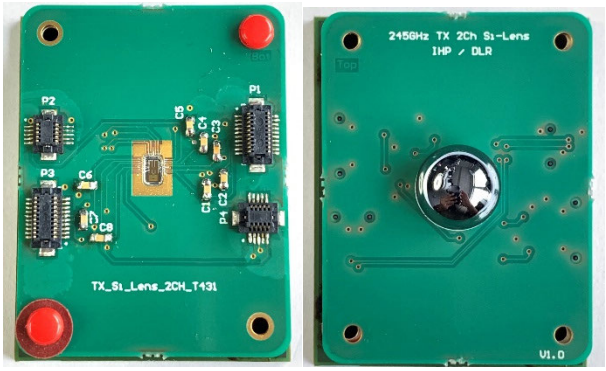

FIGURE 13. Photograph of TX adapter board with silicon lens. Left: Back with bonded TX-chip. Right: Front with Si-lens.

E. TRANSMITTER AND RECEIVER MODULES

The TX/RX chips were bonded on plug-in boards, see Fig. 13, which were mounted on baseband boards.

The baseband board contains multiple linear voltage regulators to supply all of the chips' bias voltages from a single 5 V DC supply, an amplifier to amplify the divider output of the LOs of TX and RX to the level required by the PLL, and a loop filter to determine the loop stability of the PLL circuit. The PLL device (Analog Devices ADF4169) is integrated in the baseband board. Our baseband board realizes a 2-band operation. The bands can be switched electronically by switching the LOs on and off, respectively. This allows realizing a width of the frequency band of almost 50 GHz for the spectroscopy system. An internal reference clock of 100 MHz is placed on the baseband board to allow synchronization of the four fractional-N PLLs, and it is used as an external reference clock for the experimental setup. The reference frequency for the external lock-in amplifier, which is used in case of gas spectroscopy, is derived from the 100 MHz reference clock by a fractional-N divider (Analog Devices HMC983LP5E) on the baseband board.

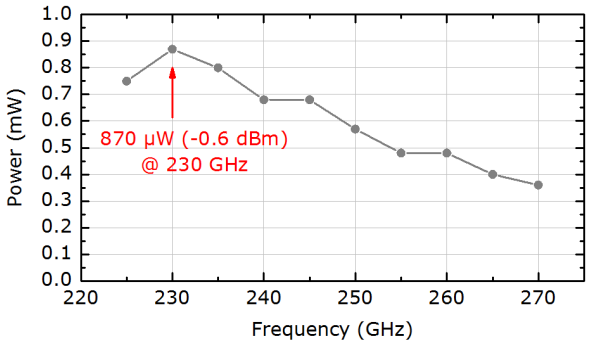

FIGURE 14. Emitted TX power measured for various frequencies with a peak value of 870 μW at 230 GHz.

F. EXPERIMENTAL RESULTS ON THE TRANSMITTER

1) RADIATED POWER OF TRANSMITTER

The TX and RX properties were characterized using the TX/RX modules described above. First, the TX emission power was determined by a Thomas Keating power meter placed at 10 cm distance to the TX module and tilted by the Brewster angle to minimize reflection losses. In thermal equilibrium, we measured the power for different frequencies as shown in Fig. 14. From the noise of the power meter signal, the uncertainty of this measurement is estimated to be ± 5 %.

We derived a peak power of 870 μW (-0.6 dBm) at 230 GHz and a decrease at higher frequencies. A 1dB decrease of the TX radiated power due to self-heating was observed after switching on the supply voltage. Considering corrections due to the (1 – 2) dB loss of the transmitted signal caused by the insertion loss of the balun, which connects the doubler output with the differential bowtie antenna, (see Fig. 4), the radiation efficiency of the antenna (65 %), and the self-heating of the TX, the measured radiated power agrees with the LO power obtained by on-wafer measurement. Thermal simulations for a radar frontend-chip on a silicon lens with nearly identical parameters (lens diameter and thermal flux of chip) revealed a chip temperature of 60 °C due to self-heating [35]. According to our simulations of the TX output power with temperature as a parameter, the TX output power decreases at 235-270 GHz by about 1 dB when the temperature is increased from 25 °C to 70 °C, see Fig. 12.

2) BEAM PROFILE OF THE TRANSMITTER

Full 2D beam profile measurements of the mmW emission radiated from the TX were performed using a Golay cell with 2 mm aperture as a power detector. It was mounted on a scanning platform and moved in a raster perpendicular to the optical axis. At a TX frequency of 240 GHz, beam scans at distances of 5 cm, 10 cm, 15 cm and 30 cm were carried out. Fig. 15 shows the normalized beam profiles. The E-field is parallel to the x-axis.

The profiles show a Gaussian-like shape with a slight double-peak, but a 2D Gaussian function still describes them appropriately (compare residuals in Fig. 16, referring to the normalized data and fit function). From the fitted

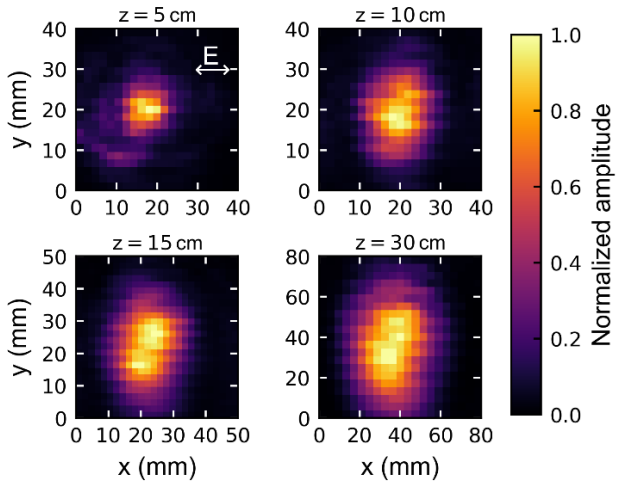

FIGURE 15. Beam profiles of the TX at different distances. The amplitudes are normalized for better illustration. The polarization of the beam is parallel to the x-axis.

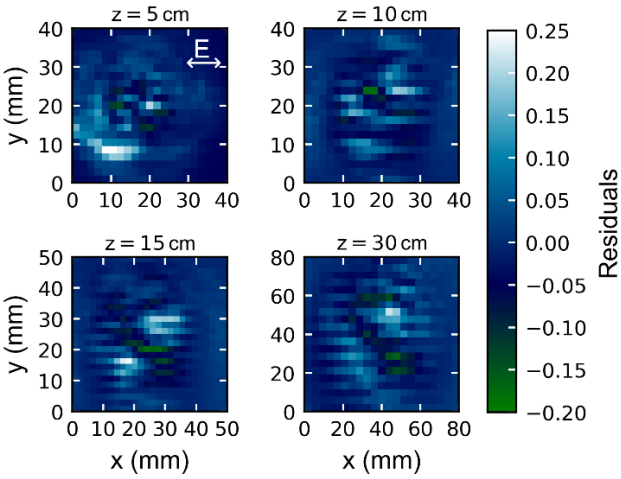

FIGURE 16. Residuals (defined as the difference between fit and measured data) of the 2D Gaussian fit to the data, with respect to the normalized data. Overall, the data are well described by the Gaussian function, despite a slight double-peak structure.

values, the beam radii w_x and w_y were calculated (compare Fig. 17). As the fitted function describes the data very well, the uncertainties of the radii are too small to be visible in this plot. By fitting Gaussian beam propagation [39], the far field divergence angles with respect to the $1/e^2$ beam radius were determined to be 5.3° in the E-plane and 8.4° in the H-plane (corresponding to 6.2° and 9.9° for full 3 dB beam widths). For a previous TX design with a double dipole antenna and without a silicon lens, see [16], we measured 17.4° and 21.8°, respectively.

From the Full Width at Half Maximum (FWHM) angles, we estimated the directivity of the antenna by using the approximation $D = 29{,}000/(\theta_x\theta_y)$ for narrow beams [40]. It results in D = 26.7 dBi at 240 GHz, which is somewhat larger than the simulated value of 24.7 dBi. Considering the

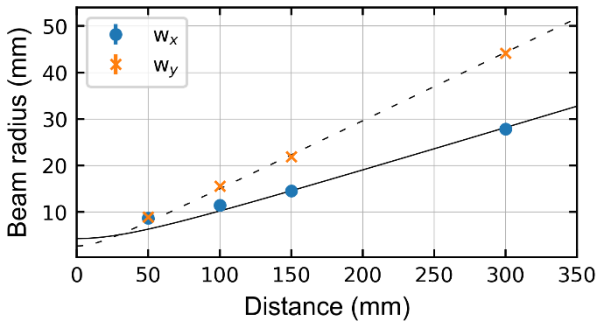

FIGURE 17. Beam radius in x- and y-direction as determined from the 2D Gaussian fit to the data. Gaussian beam propagation (solid and dashed line) yields $1/e^2$ far field divergence angles of 5.3° in E-plane and 8.4° in H-plane (FWHM: 6.2°/9.9°).

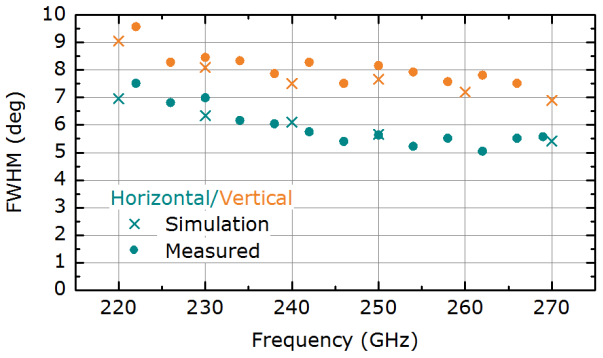

FIGURE 18. FWHM angles derived by Gaussian fits in horizontal (E-plane) and vertical (H-plane) direction. The beams get narrower with higher frequencies which agrees with the values from simulations of the antenna.

measured radiated power of - 1.5 dBm at this frequency, this would correspond to an EIRP of 25.2 dBm.

To determine the frequency dependence of the TX beam profiles, we measured angular cross sections of the beam profile in the E- and H-plane. For this measurement, we used a rotation stage to tilt the TX module from −25° to +25° in steps of 0.5° in the respective plane. The RX module was placed at a distance of 35 cm to detect the radiation through rectification of the IF power by a diode (Keysight 8472B).The large distance was chosen to reduce near field effects and the influence of the RX antenna profile.

From Gaussian fits we derived the FWHM for each frequency as shown in Fig. 18 along with the simulated values (see paragraph II. C), which agree well.

G. EXPERIMENTAL RESULTS ON THE RECEIVER

1) CONVERSION GAIN AND LINEARITY OF THE RECEIVER

To determine the conversion gain of the RX, we measured the IF power at 2150 MHz obtained from the TX at 245 GHz at different distances r to the RX (Fig. 19). We have used this relatively high IF to avoid a distortion of the IF signal due to spurious signals, which are related to the strong 1/64 frequency divider signal of the LO and its harmonics as well as mixing products of these signals with the IF signal.

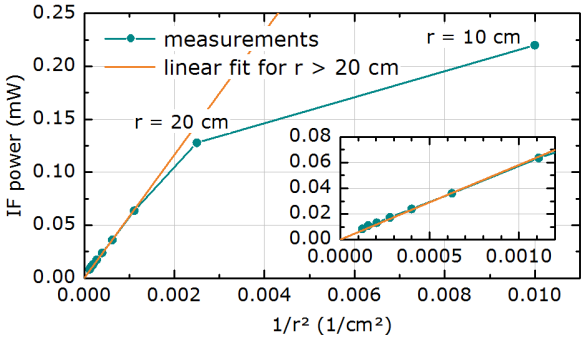

FIGURE 19. Measured IF power received at various distances from the TX. In the far field (r > 20 cm), the signal scales with $1/r^2$ as expected and a conversion gain of 6.7 dB can be derived.

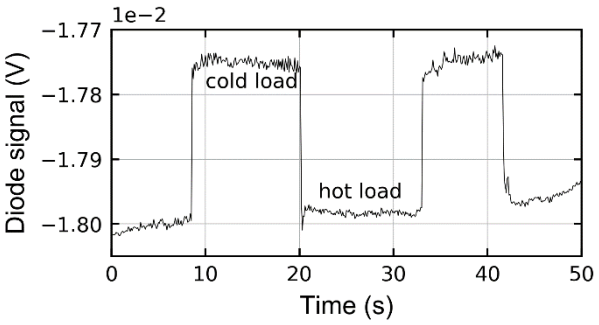

FIGURE 20. The RX noise temperature was determined with the Y-factor method. The jumps between hot and cold load correspond to a noise temperature of 20,000 K. Small drifts occurred in the measurement because of temperature changes of the RX.

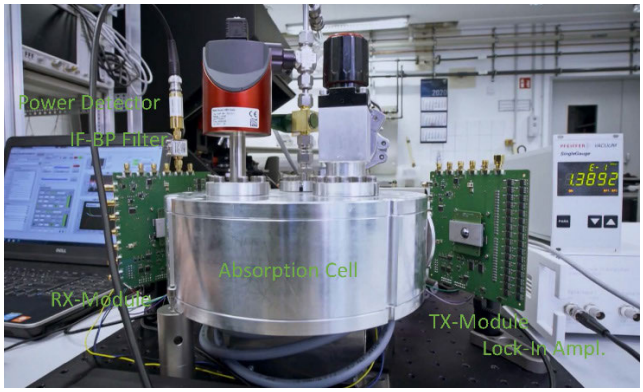

FIGURE 21. Photograph of TX and RX modules with a gas absorption cell for gas spectroscopy. The outer diameter of the absorption cell is 21.5 cm.

The IF power of the RX was measured using a single-ended IF output of the RX chip.

A $1/r^2$ dependence is observed except at short distances where nearfield conditions arise and the RX is driven in the nonlinear range due to the high power received from the TX (see below). Considering the IF power of -20.8 dBm measured at 90 cm distance, the emitted TX power of 700 μW and the directivity of 26.7 dB (see sections above), we calculated a received power of −27.4 dBm, according to the Friis transmission equation, and a conversion gain of 6.7 dB. On-wafer measurements of the RX core circuit at room temperature resulted in a conversion gain around 12 - 13 dB [30], [38]. This agrees well with our result when taking into account the simulated antenna efficiency for real antenna gain (−1.9 dB), the single-ended IF output used in the setup (−3 dB), gain decrease due to self-heating of the RX (about −2 dB), and reflection loss at the silicon lens (about −1.5 dB). Note that the simulated conversion gain decreases by about 2 dB from 25 °C to 60 °C (see Fig. 5).

The linearity of the RX was investigated by attenuating the TX power coupled into the RX by a wire grid polarizer and additional absorbers across three orders of magnitude. A strict linear behavior was noted up to an output related 1dB compression at −7 dBm IF power at 245 GHz and −9 dBm at 260 GHz.

2) NOISE PERFORMANCE OF THE RECEIVER

The double sideband (DSB) noise temperature of the RX was determined with the Y-factor method. An Eccosorb®-lined, open top container with liquid nitrogen served as cold load (77 K) and was covered with room temperature Eccosorb®for the hot load (300 K) measurements. The RX chip on the RX module was mounted 15 cm above the container to assure the loads covered the full antenna profile. A polystyrene plate and an IR filter were attached to the board to protect it from temperature fluctuations produced by evaporating nitrogen. A 90-MHz wide bandpass filter centered at 1.5 GHz (Mini Circuits VBF-1525+) and a 36 dB amplifier (Miteq AFD4-010040-20P) were connected to the IF output and the signal power was detected with a diode (Keysight 8472B). The integration time was 0.1 s.

By opening and closing the nitrogen container, several hot-cold jumps (example in Fig. 20) were recorded at 241 GHz RX frequency. Drifts occurred because the RX is temperature-sensitive and the polystyrene could not completely prevent temperature changes. The DSB noise temperature was calculated to be approximately (20,000 ± 3,000) K (18.5 dB noise figure) in average. This corresponds to a SSB noise figure of 21.5 dB and agrees well with 18 dB of NF obtained by on-wafer measurements of the RX core circuit, considering losses in the antenna and the substrate as well as heating of the chip [38].

III. GAS SPECTROSCOPY SYSTEM

A. GAS SPECTROSCOPY SETUP

The setup of the gas spectroscopy system is based on a circular multi-pass gas cell with a 1.9 m path length as presented in [41], [42]. Fig. 21 shows the TX/RX modules (baseband boards with plug-in boards) and the circular gas absorption cell in the setup for gas spectroscopy. Metal plates are attached to the adapter boards for cooling. The absorption cell has three ports for pumping, pressure sensing and letting in the gas. The IF signal is bandpass-filtered and then rectified by a diode (Keysight 8472B). For sensitive detection and

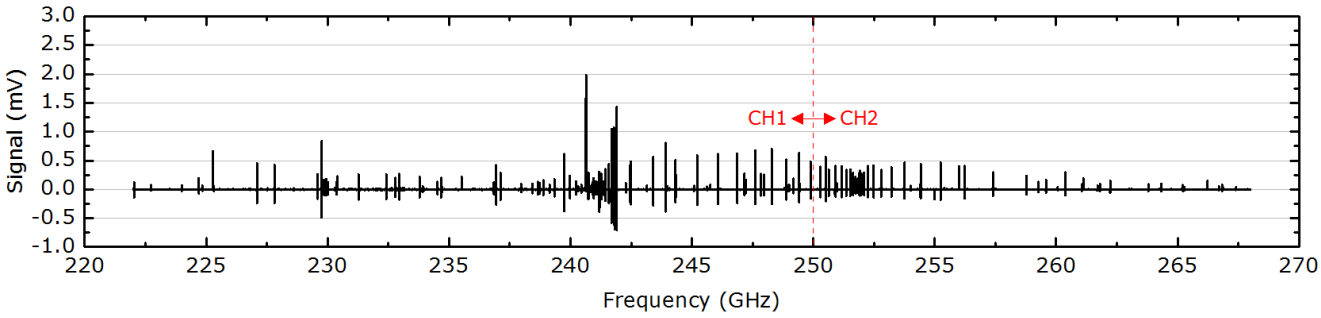

FIGURE 22. Broadband (46 GHz) spectrum of methanol measured in 15 minutes (2 ms integration time per frequency step, 100 kHz step size) with around 200 obvious absorption lines.

TABLE 1. Estimated detection limit of the system for exemplary molecular species based on the strongest absorption line between 222 and 270 GHz.

Molecule	Line intensity (cm^{-1} /(molecule·cm^{-2})	Line position (GHz)	Estimated detection limit (ppm)
Methanol	5.00E-23	241.700	10
Formaldehyde	1.61E-21	225.698	0.3
Ethanol	7.46E-23	258.485	7
Acetone	2.05E-23	269.431	24
Acetaldehyde	2.39E-22	263.004	2
Hydrogen cyanide	2.88E-20	265.886	0.02

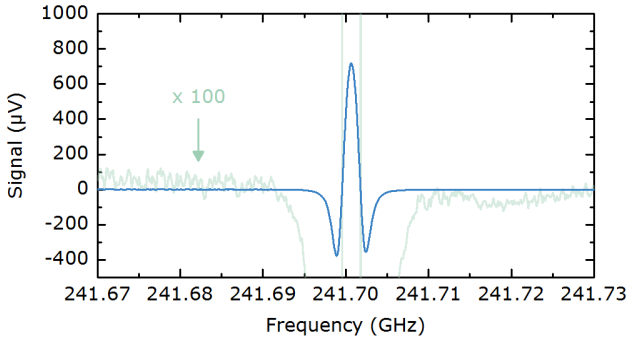

FIGURE 23. Exemplary snippet of the spectrum with a single methanol absorption line. With 2 ms integration time, an SNR of 6000 was achieved.

reducing baseline effects, we detected the second harmonic content of the frequency modulated TX signal with a lock-in amplifier (Zurich Instruments HF2LI). The TX and RX chips with Si-lenses on the TX/RX modules are placed at the entrance and exit of the gas cell. Frequency and channel settings are controlled via an I2C interface. For the full-band coverage, the LO channel is switched at 250 GHz which includes turning off the supply voltages of the inactive channel. Since both channels are emitted and received through the same antenna and the IF signal is measured through the same port, the full-band can be measured without realignment or reconnection of cables, in contrast to the system presented previously [16].

B. GAS SPECTROSCOPY RESULTS

A full-band spectrum of methanol measured at 5 Pa is shown in Fig. 22. The spectrum was acquired in a total time of approx. 15 minutes with 2 ms integration (corresponding to a ∼100 kHz step size). Around 200 absorption lines with different intensities can be recognized and assigned to rotational transitions of the methanol molecules. As an example, the strong and well isolated absorption line at 241.7 GHz with a line intensity of $5 \cdot 10^{-23}$ cm^{-1}/(molecule·cm^{-2}) reveals an SNR of 6000 (Fig. 23). Assuming a linear behavior of the signal and an SNR of one as a threshold, we can estimate a detection limit of 10 ppm/sqrt (Hz).

Due to the good coupling through the gas cell, the signal level varies by only a factor of three between minimum and maximum signal across the full-spectral band. We assume a similar behavior for the SNR across the full bandwidth, i.e. linear scaling of the SNR only with the line intensity. In this way of scaling with the strongest line in the bandwidth, we can estimate detection limits for various molecular species as summarized in Table 1.

Note that the lines of formaldehyde and hydrogen cyanide are near the edges of the frequency range, which emphasizes the advantage of the increased bandwidth of our system. With a slightly smaller bandwidth, these molecules were not detectable. Hydrogen cyanide exhibits no second line within the bandwidth and the second strongest line of formaldehyde at 264.27 GHz is weaker by a factor of 18 compared to the strongest one.

IV. DISCUSSION

The Tables 2 and 3 compare the main parameters of the TX and RX in SiGe BiCMOS described above with those of a previous version [30], and with parameters of TX- and RX-front ends in 65 nm CMOS technology [4]–[8], and TX and RX in 28 nm CMOS [11], [12], which were developed for gas spectroscopy.

We used only one antenna for the two frequency bands in the 222 – 270 GHz range in our TX/RX, which allows an easier alignment of the TX and RX in the spectroscopy

TABLE 2. Performance of transmitters for gas spectroscopy.

Parameter	MIT [4]	UTD [6], [8]	JPL [11]	Our previous work [30]	This work
Technology	65nm CMOS	65nm CMOS	28nm CMOS	0.13µm SiGe	0.13µm SiGe
Lock range (GHz)	220-330 10x 10GHz-band	208-255	180-190	243-260 (1 band) 222-270 (2 bands)	222-270 (2 bands)
Antenna	Antenna for each band, with one silicon lens	Dipole antenna	WR5 horn antenna [+] with coupler [++]	Antenna for each band	Bowtie antenna with silicon lens
EIRP (dBm)	up to 10	-19 to -11	21.6 [+++]	7 (TX) at 245GHz 18 (4xTX) at 245GHz	25.2 at 240GHz
Peak power (dBm)			0.6 [a]		3 [a]
Extern. synthesizer PLL	45-46.7GHz & 10GHz	27 -35GHz on-chip	w/o on-chip	w/o device ADF4159	w/o device ADF4169
PN (dBc/Hz), offset	-102, 1MHz [b]	-70 to -65, 300kHz	-65, 100kHz	-85, 1MHz, 240GHz *	-82 to –77 **, 1MHz -58 to -52 **, 100kHz
DC-Power (W)	1.7 [c]	1.4	0.35	0.43 [d]	0.73 [d]

[+] assuming gain of 21 dB [10], [++] CMOS-to-waveguide coupler [+++] estimated for 21 dB of antenna gain, [a] measured by probe, [b] signal generator average of 10 bands, [c] for TX+RX, [d] one band is only used, * without PLL, ** measured at 245 and 260 GHz.

TABLE 3. Performance of receivers for gas spectroscopy.

Parameter	MIT [4]	UTD [7], [8]	JPL [12]	Our previous work [16]	This work
Technology	65nm CMOS	65nm CMOS	28nm CMOS/InP hybrid	0.13µm SiGe	0.13µm SiGe
Lock range (GHz)	220-330 10x 10GHz-band	225-280	180-200	243-260 (1 band) 222-270 (2 bands)	222-270 (2 bands)
Antenna	Antenna for each band, with one silicon lens	Dipole antenna	Horn antenna [+]	Antenna for each band	Bowtie antenna with silicon lens
Directivity (dBi)	average 10.1	-1 to 2 [a]	21 [+]	7 [a]	26.7 at 240 GHz
NF of RX (dB) (SSB)	14.6 – 19.5 [b]	13.9 – 19 [c]	8.3 -9.5 [*]	18 at 240GHz [b]	18 at 240 GHz [b] 21.5 at 240 GHz [d]
IF-output	10 for 10 bands	1	1	2 for 2 bands	1 for 2 bands
Ext. Synthesizer PLL	45-46.7GHz&10GHz	30.4-34.8GHz on-chip	w/o on-chip	w/o device ADF4159	w/o device ADF4169
DC Power (W)	1.7 [e]	0.042 [f]	0.615 [g]	0.73	0.93

[+] assuming gain of 21 dB and low loss, [*] estimated from noise temperature, [a] simulated antenna gain, [b] measured by gain method, [c] at 210 - 305 GHz, [d] measured by Y-factor method including antenna, [e] for TX+RX, [f] without quadrupler and LO driver, [g] 0.1 W for InP LNA and 0.515 W for CMOS RX.

system setup compared to our previous TX- and RX-chips with two integrated LBE antennas [30], and compared to the 10 antennas on a silicon lens developed by MIT (Massachusetts Institute of Technology) [4].

We applied a dual-band architecture for the LO, because IHP's 0.13 μm SiGe BiCMOS technology does not allow designing a wide-band VCO with a center frequency of 120 GHz and a tuning range of 50 GHz.

TX/RX chips in 65 nm CMOS are reported by UTD (University of Texas at Dallas). They have a common frequency range of 225 - 255 GHz and are used for gas spectroscopy [9]. The 200-280 GHz TX front-end consists of an up-conversion mixer and an on-chip antenna, which amplify and mix an input signal at 90-150 GHz with a LO-signal at 110 −130 GHz to generate the TX signal [8]. The RX front-end down-converts a 225-280 GHz RF input to 18.5 GHz IF frequency [8]. The RX and TX include an on-chip dipole antenna with a simulated peak gain of −1 to 2 dBi [7].

The 65nm CMOS based system with its 10 × 10 GHz spectrum acquisition, presented by MIT, uses 10 antennas on a single silicon lens, [4], [5], and generates 10 IF-outputs of corresponding RX-units, making baseband processing more challenging compared to our RX with only one IF-output. The radiation pattern of the CMOS TX was measured at 220-330 GHz. An average directivity of 10.1 dBi was obtained for the on-chip antenna with silicon lens [4].

A 180 GHz pulsed CMOS TX has been designed by JPL (Jet Propulsion Laboratory) for planetary in-situ molecular sensing applications [11]. A 183-GHz CMOS/InP hybrid heterodyne-spectrometer has been realized by JPL for spaceborne atmospheric remote sensing applications [12]. An external InP low noise amplifier is added at the front-end to provide the required RX sensitivity for remote sensing. These CMOS TX and RX use a horn antenna [11], [12].

Using the directivity to estimate the conversion gain by the Friis equation, we obtained an agreement with our on-wafer measurement results for the conversion gain. Note that the estimated directivity of 26.7 dBi is somewhat larger than the simulated one of 24.7 dBi, probably caused by the considered approximations. Either way, our bowtie antenna with silicon lens reveals a considerably higher directivity (by about 15 dB) compared to the antennas implemented in the CMOS TX/RX system of MIT and to our previous systems.

TABLE 4. Performance of gas spectroscopy setups.

Parameter	MIT [5]	UTD [9]	This work
Technology	65nm CMOS	65nm CMOS	0.13µm SiGe
Range (GHz)	220-330	225-255	222-270
Length of cell (m)	0.7	1	1.9
Gas	OCS [a]	Ethanol	Methanol
Line freq. (GHz)	279.685	242.626	241.7
Gas pressure (Pa)	10	0.3	5
Peak absorption a	0.94	0.05**	0.16**
SNR	29,000	3	6,000
Integr. time τ (s)	1	8	0.002
Minimum detect. absorption* (τ=1s)	3e-5	0.05	1e-6

[a] OCS - carbonyl sulfide, * Estimated through $a \cdot \sqrt{(\tau/1\ \mathrm{s})}$ / SNR, ** Estimated from simulations based on the JPL molecular spectroscopy data base.

Because the emitted output power of our TX (e.g. −0.6 dBm at 230 GHz) is comparable with the one of the CMOS TX of MIT, the considerably higher EIRP of our TX is related mainly to the higher directivity of its antenna, as also observed for the TX of JPL.

At the TX and RX frequencies used in our gas spectroscopy setup, the RX still works in the linear regime (with an IF-power of −9 dBm at 245 GHz, and an output related 1 dB compression of −7 dBm), indicating that the TX output power could still be further increased. For our RX with its bowtie antenna, we obtained a SSB noise figure of 21.5 dB by the Y-factor method, which agrees with the SSB value of 18 dB obtained by the gain method for this RX circuit without antenna [38], indicating a low contribution of noise related to the antenna in case of antenna with silicon lens.

As a benchmark for our TX/RX systems, we determined the SNR value of the CH_3OH absorption line at 241.7 GHz at a pressure of 5 Pa. For our TX- and RX-chips with bowtie antenna with silicon lens, an SNR of 6000 for this line was achieved. Using our previous TX and RX with LBE antenna, an SNR of only 2160 was observed with similar parameters for a methanol absorption line of similar intensity at 247.6 GHz [30]. However, when we replaced the TX by a 4 x TX-array with a higher EIRP (18 dBm at 245 GHz), we observed an SNR of 4660 under similar conditions [22].

The presented TX/RX spectroscopy system realizes a minimum detectable absorption for gas detection which is at least by factor 30 lower compared to previously reported wide-band TX/RX systems (see Table 4). Our simple estimation is based on the following assumptions: First, we assume that the signal scales linearly with the peak absorption a (as given in the publication or estimated from simulations). Second, the SNR scales with the integration time by $\sqrt{\tau}$. Thus, we can estimate a minimum detectable absorption (for which SNR=1) normalized to 1 s integration time by $a_{\mathrm{min,1s}} = a \cdot \sqrt{(\tau/1\ \mathrm{s})}/\mathrm{SNR}$.

The sensitivity of the spectroscopy system can be increased when using a TX with higher output power. Previously, we showed that the SNR increases with the square root of the TX power [22]. For comparison, we obtained an SNR of 7900 with comparable measurement parameters under similar conditions utilizing a commercial TX/RX system from Virginia Diodes Inc. (WR3.4AMC-I and WR3.4MixAMC-I with diagonal horn antennas) [30].

V. CONCLUSION

A TX and a RX in 0.13 μm SiGe BiCMOS technology with bowtie-antenna and silicon lens were developed for gas spectroscopy at 222-270 GHz. The frequency range is realized by combining two frequency bands, which can be switched electronically for dual-band operation. The high directivity of the bowtie-antenna increases the performance of the TX/RX system significantly compared to previously reported systems. The performance was demonstrated in a gas spectroscopy setup. The estimated detection limits range from sub-ppm to a few ppm, depending on the absorption strength of the molecular transitions.

The TX and RX will be further developed for our gas spectroscopy system in order to improve its sensitivity. This may be achieved by increasing the TX output power and minimizing the noise.

REFERENCES

[1] I. Medvedev, C. Neese, G. Plummer, and F. De Lucia, "Submillimeter spectroscopy for chemical analysis with absolute specificity," *Opt. Lett.*, vol. 35, no. 10, pp. 1533–1535, May 2010.
[2] C. F. Neese, I. R. Medvedev, G. M. Plummer, A. J. Frank, C. D. Ball, and F. C. De Lucia, "Compact submillimeter/terahertz gas sensor with efficient gas collection, preconcentration, and ppt sensitivity," *IEEE Sensors J.*, vol. 12, no. 8, pp. 2565–2574, Aug. 2012.
[3] A. M. Fosnight, B. L. Moran, and I. R. Medvedev, "Chemical analysis of exhaled human breath using a terahertz spectroscopic approach," *Appl. Phys. Lett.*, vol. 103, no. 13, Sep. 2013, Art. no. 133703.
[4] C. Wang and R. Han, "Dual-terahertz-comb spectrometer on CMOS for rapid, wide-range gas detection with absolute specificity," *IEEE J. Solid-State Circuits*, vol. 52, no. 12, pp. 3361–3372, Dec. 2017.
[5] C. Wang, B. Perkins, Z. Wang, and R. Han, "Molecular detection for unconcentrated gas with ppm sensitivity using dual-THz-comb spectrometer in CMOS," *IEEE Trans. Biomed. Circuits Syst.*, vol. 12, no. 3, pp. 709–721, Jun. 2018.
[6] N. Sharma, Q. Zhong, Z. Chen, W. Choi, J. P. Mcmillan, C. F. Neese, R. Schueler, I. Medvedev, F. De Lucia, and K. O, "200–280GHz CMOS RF front-end of transmitter for rotational spectroscopy," in *Proc. IEEE Symp. VLSI Technol.*, Jun. 2016, pp. 1–2, doi: 10.1109/VLSIT.2016.7573400.
[7] Q. Zhong, W. Choi, C. Miller, R. Henderson, and K. O. Kenneth, "25.2 A 210-to-305GHz CMOS receiver for rotational spectroscopy," in *IEEE Int. Solid-State Circuits Conf. (ISSCC) Dig. Tech. Papers*, Jan. 2016, pp. 426–427, doi: 10.1109/ISSCC.2016.7418089.
[8] N. Sharma, Q. Zhong, W. Choi, J. Zhang, Z. Chen, Z. Ahmad, I. R. Medvedev, D. J. Lary, H. J. Nam, P. Raskin, and I. Kim, "Complementary metal oxide semiconductor integrated circuits for rotational spectroscopy," *Proc. SPIE*, vol. 11390, May 2020, Art. no. 113900K.
[9] I. R. Medvedev, R. Schueler, J. Thomas, O. Kenneth, H.-J. Nam, N. Sharma, Q. Zhong, D. J. Lary, and P. Raskin, "Analysis of exhaled human breath via terahertz molecular spectroscopy," in *Proc. 41st Int. Conf. Infr., Millim., THz waves (IRMMW-THz)*, Sep. 2016, pp. 1–2, doi: 10.1109/IRMMW-THz.2016.7758450.
[10] *Products: Compact Transmitter Modules, Compact Receiver Modules; VDI Application Note: VDI_Feedhorn_Summary_2020.05.04*. Accessed: Sep. 6, 2021. [Online]. Available: http://www.vadiodes.com
[11] D. Nemchick, H. Hakopian, B. Drouin, A. Tang, M. Alonso-delPino, G. Chattopadhyay, and F. Chang, "180-GHz pulsed CMOS transmitter for molecular sensing," *IEEE Trans. THz Sci. Technol.*, vol. 11, no. 5, pp. 469–476, Sep. 2021, doi: 10.1109/TTHZ.2021.3085138.

[12] Y. Kim, Y. Zhang, T. J. Reck, D. J. Nemchick, G. Chattopadhyay, B. Drouin, M.-C. F. Chang, and A. Tang, "A 183-GHz InP/CMOS-hybrid heterodyne-spectrometer for spaceborne atmospheric remote sensing," *IEEE Trans. THz Sci. Technol.*, vol. 9, no. 3, pp. 313–334, May 2019.
[13] A. Ali, J. Yun, M. Kucharski, H. J. Ng, D. Kissinger, and P. Colantonio, "220-360-GHz broadband frequency multiplier chains (x8) in 130-nm BiCMOS technology," *IEEE Trans. Microw. Theory Techn.*, vol. 68, no. 7, pp. 2701–2715, Jul. 2020.
[14] A. Ali, "168-195 GHz power amplifier with output power larger than 18 dBm in BiCMOS technology," *IEEE Access*, vol. 8, pp. 79299–79309, 2020, doi: 10.1109/ACCESS.2020.2990681.
[15] M. H. Eissa, A. Malignaggi, R. Wang, M. Elkhouly, K. Schmalz, A. C. Ulusoy, and D. Kissinger, "Wideband 240-GHz transmitter and receiver in BiCMOS technology with 25-Gbit/s data rate," *IEEE Journ. Solid-State Circuits*, vol. 53, no. 9, pp. 2532–2542, Sep. 2018.
[16] P. Rodriguez-Vazquez, J. Grzyb, B. Heinemann, and U. R. Pfeiffer, "A QPSK 110-Gb/s polarization-diversity MIMO wireless link with a 220–255 GHz tunable LO in a SiGe HBT technology," *IEEE Trans. Microw. Theory Techn.*, vol. 68, no. 9, pp. 3834–3851, Sep. 2020.
[17] S. Lee, S. Hara, T. Yoshida, S. Amakawa, R. Dong, A. Kasamatsu, J. Sato, and M. Fujishima, "An 80-Gb/s 300-GHz-band single-chip CMOS transceiver," *IEEE J. Solid-State Circuits*, vol. 54, no. 12, pp. 3577–3588, Dec. 2019.
[18] S. Thomas, C. Bredendiek, and N. Pohl, "A SiGe-based 240-GHz FMCW radar system for high-resolution measurements," *IEEE Trans. Microw. Theory Techn.*, vol. 67, no. 11, pp. 4599–4609, Nov. 2019.
[19] X. Yi, C. Wang, X. Chen, J. Wang, J. Grajal, and R. Han, "A 220-to-320-GHz FMCW radar in 65-nm CMOS using a frequency-comb architecture," *IEEE J. Solid-State Circuits*, vol. 56, no. 2, pp. 327–339, Feb. 2021.
[20] K. Schmalz, Y. Mao, J. Borngräber, P. Neumaier, and H. Hübers, "Tunable 245 GHz transmitter and receiver in SiGe technology for gas spectroscopy," *Electron. Lett.*, vol. 50, no. 12, pp. 881–882, Jun. 2014.
[21] K. Schmalz, P. Neumaier, J. Borngraber, W. Debski, and H.-W. Hubers, "245 GHz transmitter and receiver in SiGe for gas spectroscopy," in *Proc. 39th Int. Conf. Infr., Millim., THz waves (IRMMW-THz)*, Sep. 2014, pp. 1–2.
[22] K. Schmalz, J. Borngräber, W. Debski, M. Elkhouly, R. Wang, P. Neumaier, and H.-W. Hübers, "245-GHz transmitter array in SiGe BiCMOS for gas spectroscopy," *IEEE Trans. THz Sci. Technol.*, vol. 6, no. 2, pp. 318–327, Mar. 2016.
[23] K. Schmalz, R. Wang, W. Debski, H. Gulan, J. Borngräber, P. Neumaier, and H.-W. Hübers, "245 GHz SiGe sensor system for gas spectroscopy," *Int. J. Microw. Wireless Technol.*, vol. 7, nos. 3–4, pp. 271–278, Jun. 2015.
[24] K. Schmalz, R. Wang, J. Borngraber, W. Debski, W. Winkler, and C. Meliani, "245 GHz SiGe transmitter with integrated antenna and external PLL," in *IEEE MTT-S Int. Microw. Symp. Dig.*, Jun. 2013, pp. 1–4.
[25] K. Schmalz, J. Borngraber, B. Heinemann, H. Rucker, and J. C. Scheytt, "A 245 GHz transmitter in SiGe technology," in *Proc. IEEE Radio Freq. Integr. Circuits Symp.*, Jun. 2012, pp. 195–198.
[26] K. Schmalz, J. Borngraber, P. Neumaier, H.-W. Hubers, and D. Kissinger, "Sensor system in SiGe BiCMOS at 245 and 500 GHz for gas spectroscopy," in *Proc. IEEE 16th Topical Meeting Silicon Monolithic Integr. Circuits RF Syst. (SiRF)*, Jan. 2016, pp. 70–72.
[27] K. Schmalz, J. Borngraber, P. Neumaier, N. Rothbart, D. Kissinger, and H.-W. Hubers, "Gas spectroscopy system at 245 and 500 GHz using transmitters and receivers in SiGe BiCMOS," in *Proc. Global Symp. Millim. Waves (GSMM) ESA Workshop Millimetre-Wave Technol. Appl.*, Jun. 2016, pp. 1–4.
[28] N. Rothbart, J. Borngräber, S. B. Yilmaz, D. Kissinger, and H. W. Hübers, "Gas spectroscopy system with transmitters and receivers in SiGe BiCMOS for 225-273 GHz," *Proc. SPIE*, vol. 10439, Oct. 2017, Art. no. 1043902.
[29] K. Schmalz, N. Rothbart, P. F.-X. Neumaier, J. Borngraber, H.-W. Hubers, and D. Kissinger, "Gas spectroscopy system for breath analysis at mm-wave/THz using SiGe BiCMOS circuits," *IEEE Trans. Microw. Theory Techn.*, vol. 65, no. 5, pp. 1807–1818, May 2017.
[30] K. Schmalz, N. Rothbart, M. H. Eissa, J. Borngräber, D. Kissinger, and H.-W. Hübers, "Transmitters and receivers in SiGe BiCMOS technology for sensitive gas spectroscopy at 222–270 GHz," *AIP Adv.*, vol. 9, no. 1, Jan. 2019, Art. no. 015213.
[31] A. Babakhani, G. Xiang, A. Komijani, A. Natarajan, and A. Hajimiri, "A 77-GHz phased-array transceiver with on-chip antennas in silicon: Receiver and antennas," *IEEE J. Solid-State Circuits*, vol. 41, no. 12, pp. 2795–2806, Dec. 2006.
[32] J. Grzyb, K. Statnikov, N. Sarmah, B. Heinemann, and U. R. Pfeiffer, "A 210–270-GHz circularly polarized FMCW radar with a single-lens-coupled SiGe HBT chip," *IEEE Trans. THz Sci. Technol.*, vol. 6, no. 6, pp. 771–783, Nov. 2016.
[33] K. Statnikov, J. Grzyb, B. Heinemann, and U. R. Pfeiffer, "160-GHz to 1-THz multi-color active imaging with a lens-coupled SiGe HBT chip-set," *IEEE Trans. Microw. Theory Techn.*, vol. 63, no. 2, pp. 520–532, Feb. 2015.
[34] R. Han and E. Afshari, "A CMOS high-power broadband 260-GHz radiator array for spectroscopy," *IEEE J. Solid-State Circuits*, vol. 48, no. 12, pp. 3090–3104, Dec. 2013.
[35] B. Goettel, W. Winkler, A. Bhutani, F. Boes, M. Pauli, and T. Zwick, "Packaging solution for a millimeter-wave system-on-chip radar," *IEEE Trans. Compon., Packag., Manuf. Technol.*, vol. 8, no. 1, pp. 73–81, Jan. 2018.
[36] Accessed: Sep. 6, 2021. [Online]. Available: /services/research-and-prototyping-service/mpw-prototyping-service/sigec-bicmos-technologies
[37] K. Schmalz, J. Borngraber, B. Heinemann, H. Rucker, and J. C. Scheytt, "A 245 GHz transmitter in SiGe technology," in *Proc. IEEE Radio Freq. Integr. Circuits Symp.*, Jun. 2012, pp. 195–198, doi: 10.1109/RFIC.2012.6242262.
[38] M. H. Eissa, A. Awny, M. Ko, K. Schmalz, M. Elkhouly, A. Malignaggi, A. C. Ulusoy, and D. Kissinger, "A 220–275 GHz direct-conversion receiver in 130-nm SiGe:C BiCMOS technology," *IEEE Microw. Wireless Compon. Lett.*, vol. 27, no. 7, pp. 675–677, Jul. 2017.
[39] P. F. Goldsmith, *Quasioptical Systems*. Hoboken, NJ, USA: Wiley, 1998.
[40] J. E. Hill, "Gain of directional antennas," Watkins-Johnson Company, Palo Alto, CA, USA, Tech. Notes, Jul./Aug. 1976, vol. 3, no. 4.
[41] N. Rothbart, O. Holz, R. Koczulla, K. Schmalz, and H.-W. Hübers, "Analysis of human breath by millimeter-wave/terahertz spectroscopy," *Sensors*, vol. 19, no. 12, p. 2719, Jun. 2019, doi: 10.3390/s19122719.
[42] N. Rothbart, K. Schmalz, and H.-W. Hubers, "A compact circular multipass cell for millimeter-wave/terahertz gas spectroscopy," *IEEE Trans. THz Sci. Technol.*, vol. 10, no. 1, pp. 9–14, Jan. 2020.

KLAUS SCHMALZ received the Ph.D. degree in physics, in 1978. He worked in the field of silicon semiconductor technologies and research for some time and has expertise in the area of thermally induced defects and characterization of Si/SiGe structures. After training in RF circuit design at UCLA, Los Angeles, from 1998 to 1999, he changed his scientific focus to RF analog circuit design. He is currently with IHP, Frankfurt (Oder). He has authored and coauthored more than 100 papers. His current research interests include the design of SiGe BiCMOS analog circuits for wireless communication with emphasis on RF front-ends for different standards and mm-wave circuits for sensor applications.

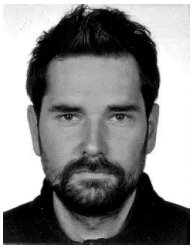

NICK ROTHBART received the Master of Science degree in physics from Humboldt-Universität zu Berlin, in 2011, and the Dr. rer. nat. degree in physics from Technische Universität Berlin, in 2015, for his work on security-relevant terahertz imaging and spectroscopy. This work was accomplished at the German Aerospace Center (DLR), Berlin, and supported by a scholarship and a membership at Helmholtz Research School on Security Technologies (HRSST). From 2014 to 2015, he was with the Federal Institute for Materials Research and Testing (BAM). Since 2015, he has been involved in mmW/THz gas spectroscopy at DLR and Humboldt-Universität zu Berlin.

ALEXANDRA GLÜCK was born in Karlsruhe, Germany, in 1995. She received the B.Sc. degree in physics from the University of Freiburg, Freiburg, Germany, in 2016, and the M.Sc. degree in physics from Humboldt-Universität zu Berlin, Berlin, Germany, in 2019. She is currently pursuing the Ph.D. degree with the German Aerospace Center, Berlin. Her work focuses on high resolution gas spectroscopy at GHz frequencies.

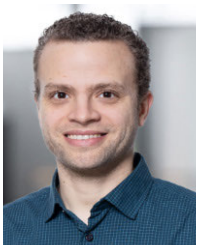

MOHAMED HUSSEIN EISSA (Member, IEEE) received the B.Sc. degree in electrical engineering from Ain Shams University, Cairo, Egypt, in 2009, the M.Sc. degree in electronics and communications from The American University in Cairo, in 2014, and the Ph.D. degree from the Technical University of Berlin, in 2019. For two years, he worked with Silicon Vision LLC., Cairo, involved in the design of ASICs for low power bluetooth communication standard. From 2011 to 2014, he joined Hittite Microwave, Cairo, working in the design of transceivers for point to point communication. Since October 2014, he has been working with IHP, Germany, as a Research Scientist with the Circuit Design Department. His research interests include RF and mm-wave circuit designs for communication and radar applications.

THOMAS MAUSOLF received the Diploma degree in electrical and information technology from Brandenburg University of Applied Science, in 2005. Since 2006, he has been working with the Technology Department, IHP. From 2006 to 2018, he was leading the Design Kit Group, IHP, developing various process design kits (PDK) for IHPs 0.25 and 0.13 μm high performance SiGe BiCMOS technologies. Since 2018, he has been leading the High Frequency Characterization Laboratory, IHP, becoming a Specialist for the characterization of high frequency ICs for the mm-wave up to the THz frequency range.

ESREF TURKMEN received the B.S. degree in electronics and communication engineering from Istanbul Technical University, Istanbul, Turkey, in 2015, and the M.S. degree in electronics engineering from Sabanci University, Istanbul, in 2018. He is currently pursuing the Ph.D. degree in cooperation with Karlsruhe Institute of Technology, Karlsruhe, Germany. In 2018, he joined Silicon Radar GmbH, Frankfurt (Oder), as an RFIC Designer. He has written several articles published in IEEE publications. His current research interests include millimeter-wave circuit and antenna design for radar and imaging applications. He was a recipient of the IEEE MTT-S Undergraduate/Pre-Graduate Scholarship Award for his work in voltage controlled-oscillators, in 2015, and won the First Place in the IEEE IMS Student Design Competition on Tunable X-Band Oscillator using Planar Resonator, in 2015.

SELAHATTIN BERK YILMAZ received the B.Sc. degree in electronics and communication engineering from Izmir Institute of Technology, Izmir, Turkey, in 2012, and the M.Sc. degree in sensor systems technology from Karlsruhe University of Applied Sciences, Karlsruhe, Germany, in 2015. In 2014, he joined Endress and Hauser Group, Ulm, Germany, for his master thesis focused on PCB design for radar level measurements. Since 2015, he has been with Silicon Radar GmbH, Frankfurt (Oder), Germany, as a PCB and a Sensor Systems Designer. He is currently the Head of hardware and also focusing on semiconductor package designs for MMICs. His research interests include radar sensors for object/presence detection and localization for industrial applications, such as robotics, material inspection, level measurement, and mobility. He is also interested in advanced semiconductor packaging technologies.

HEINZ-WILHELM HÜBERS received the Diploma and Dr. rer. nat. degrees in physics from Universität Bonn, Germany, in 1991 and 1994, respectively. From 1991 to 1994, he was with Max-Planck-Institut für Radioastronomie, Bonn, Germany. In 1994, he joined Deutsches Zentrum für Luft- und Raumfahrt (German Aerospace Center, DLR), Berlin, Germany, where he became the Head of department, in 2001. From 2009 to 2014, he was a Professor of experimental physics at Technische Universität Berlin, Germany, and the Head of the Department of Experimental Planetary Physics, DLR. In 2014, he became the Director of DLR's Institute of Optical Sensor Systems and a Professor at Humboldt-Universität zu Berlin. His research interests include THz physics and spectroscopy, particularly in THz systems for astronomy, planetary research, and security. He has received the Innovation Award on Synchrotron Radiation, in 2003, and Lilienthal Award, in 2007.